Chapter IV

Photoconductive attributes of nanostructured WS_2 based resistive system coupled with $^{1}/_{f}$ dependent noise

"To know what you know and what you do not know, that is true knowledge"

- Confucius

4.1 Introduction

As discussed in *Chapter I*, transition metal dichalcogenides (TMDCs) have intriguing physical, optical, electronic, and optoelectronic properties. For-instance, at monolayer limit, they are direct band gap semiconductors and they exhibit high quantum luminescence efficiency. This would facilitate high photo absorption coefficient and efficient electron-hole (*e-h*) pair generation for effective photoconduction under photo-excitation. In addition to monolayers, few-layer TMDCs also show considerable optical properties [1]. As such, various laser-irradiated investigation on TMDC-based electronic systems were performed for different applications. It was observed that [2], few-layer MoS_2 phototransistor can efficiently generate photocurrent under red, green, and blue laser irradiation. Similarly, Perea-López *et al.* [3] has reported large photocurrent for higher energetic laser irradiation. Likewise, Choi *et al.* [4] has reported higher photocurrent in multilayer MoS_2 nanosheets than that in monolayer. Thus, copious research articles have elucidated laser-induced enhancement of current in TMDC-based electronic systems. However, very few has reported laser-induced enhancement in current fluctuation or noise. Although noise is considered unwanted in many applications, it is the heart of stochastic resonance applications. Stochastic resonance is a phenomenon where a threshold value of noise is used to extract the information from a weak signal [5]. The first stochastic resonance phenomenon was observed in a Schmitt trigger circuit [6]; thereafter, it was reported to be observed in many electronic devices, such as superconducting quantum interference devices (SQUID) [7], field-effect transistors (FETs), [8–10] photodetectors [5, 11, 12] etc. Generally, stochastic resonance devices engage external noise generators to detect weak signals [13,14]. However, these noise generators are bulky and they put limit to the dimensionality and applicability of the system. Accordingly, researchers have designed experiments for fabricating alternative noise generators [15,16]. As such, Bao *et al*. [15] used laser irradiated technique to generate current noise in self doped polyaniline to realize artificial noise-stimulated microelectronic system. Inspired by such futuristic application of noise, an attempt has been made to fabricate a noise-coupled TMDC system. Then the photoconductive attribute of TMDCs was used to amplify the generated noise using laser-irradiation.

Thus, in this chapter, we have described the fabrication of a TMDC-based noise-coupled resistive system. To fabricate the same, bulk WS_2 flakes were first exfoliated via a green route. Then, finger-like Cu electrodes were fabricated using the same process and maintaining the same dimensions as discussed in *Chapter III*. The fabrication of finger-like electrodes was followed by drop-casting WS_2 nanosheets on it. However, unlike *Chapter III*, in this study, we implemented post-fabrication processes. In order to confirm the fabrication of the noise-coupled resistive system, electrical characterization of the system was performed at every fabrication step. Furthermore, photoconductive property of the resistive unit was assessed by performing *in situ* electrical characterization while irradiating the unit with different laser sources.

4.2 Experimental Details

Micron-sized WS_2 flakes with a purity of 99.9% (*Sigma Aldrich*®) were dispersed in a mixture of isopropanol (IPA) and acetone in a 1:4 ratio. The final concentration of WS_2 flakes in the solvent was 1.5 mg mL^{-1}. Then, the dispersed WS_2 was sonicated for 6 h with periodic shaking for the first 2 h and centrifuged at 3000 rpm to obtain the nanosheets. The exfoliation steps are presented in **Fig. 2.1** of *chapter II*. Then ~100 µL of liquid-dispersed as-synthesized nanosheets was drop-casted onto Cu electrodes as demonstrated in **Fig. 3.1** of *chapter III*. Each drop-casting step was followed by 9 h of vacuum drying. In the post fabrication process, the unit was further dried for 12 h, also termed as *hard drying*. Following these methods, several resistive units were prepared for the investigation. The electrical characterizations after each drying process and during the laser irradiation were recorded using a Keithley 2400® source meter. The arrangement for laser irradiation on the WS_2 based resistive unit is shown in **Fig 4.1**. This arrangement is maintained for all

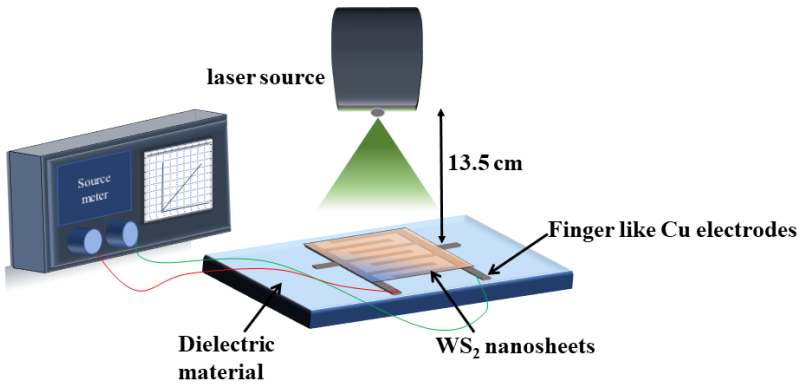

Fig.4.1. Schematic of the experimental set-up for investigation of laser irradiated effects on WS_2 nanosheets based resistive unit.

the laser sources and resistive units. The crystallographic information of the as-synthesized nanostructure was obtained from X-ray diffraction (XRD) spectra using a Rigaku Miniflex goniometer. The morphology of the as-synthesized nanostructures was obtained using SEM (by JEOL). The molecular vibrational characteristics were obtained using Raman spectrometer by RENISHAW, where the excitation wavelength was 514 nm (Ar^+ laser).

4.3 Results and discussions

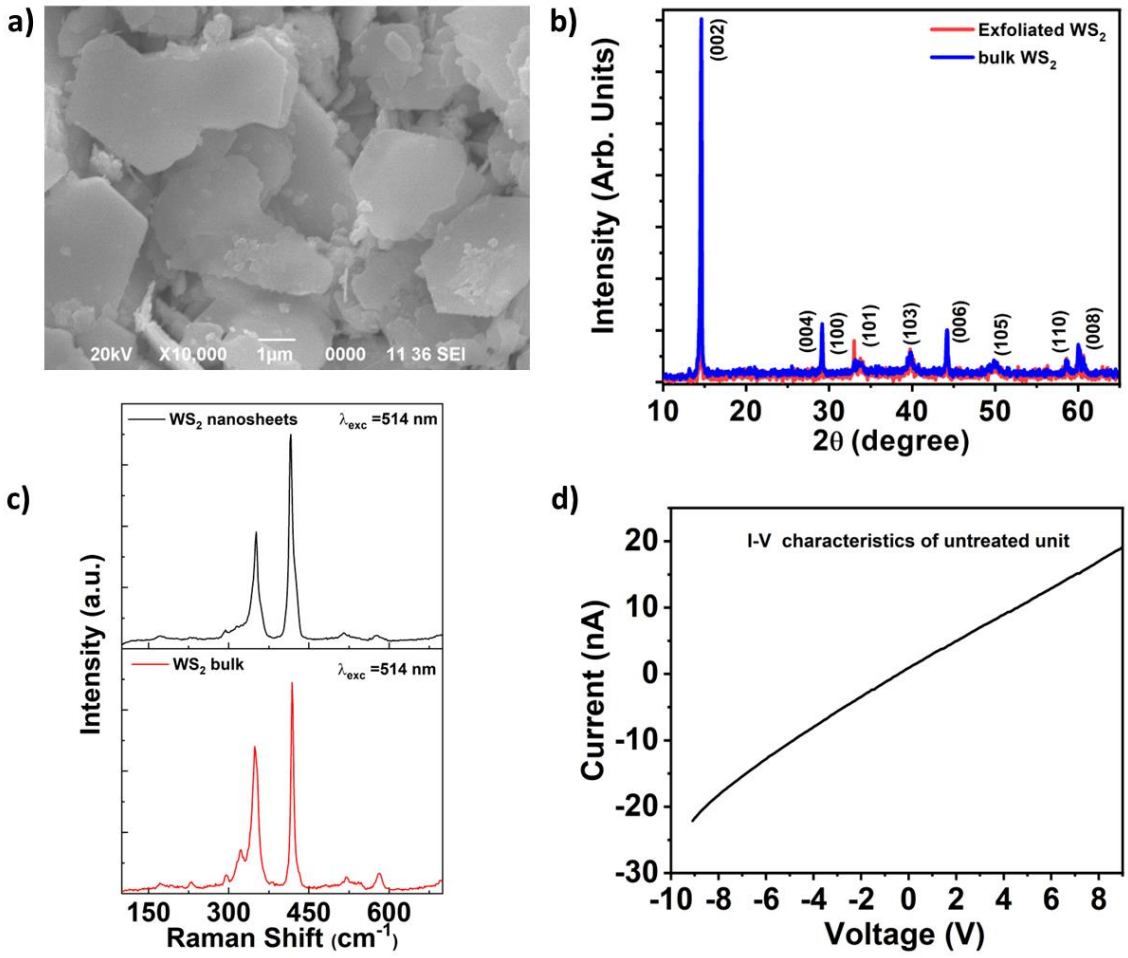

Fig.4.2. **(a)** SEM micrograph of WS_2 nanosheets. The lateral size of the sheets was of the order of μm, whereas the thickness was in nm **(b)** XRD spectra of both bulk and WS_2 nanosheets **(c)** Raman spectra of WS_2 bulk and nanosheets and **(d)** current-voltage (*I*–*V*) characteristics of the resistive unit before the introduction of noise.

4.3.1 Morphological and crystallographic analysis

The micrograph of the nanostructured WS_2 is shown in **Fig. 4.2(a)**. The lateral size was of the order of μm, while width was in nm range. The XRD spectra (**Fig. 4.2(b)**) represents the hexagonal crystallographic *(2H)* structure of WS_2 crystal (JCPDS-84-1398). The

strongest peak in the XRD spectra is observed at 14.56°. It is the standard diffraction peak of WS_2 crystal, which corresponds to diffraction from (002) crystallographic plane. This plane lies along the *c*-axis of the hexagonal crystal structure. The other diffraction peaks correspond to different other crystallographic planes, as shown in **Fig. 4.2(b)**. The intensities of the peaks observed for the exfoliated crystals were less than that of the bulk. This reduction in intensity profile was distinct in the case of the peak corresponding to the (002) crystallographic plane. This observation confirms the de-stacking of the layered crystals. Using single line fitting along the (002) crystallographic peak, the average crystallite size of the bulk and exfoliated sheets was calculated and found to be 61.77 ±0.01 nm and 40.87 ± 0.01 nm, respectively. The crystallite size of the exfoliated sheets was smaller than that of the bulk, suggesting the exfoliation.

4.3.2 Raman Analysis

The Raman spectra of the bulk and exfoliated sheets are shown in **Fig. 4.2(c)**. The phonon modes of the exfoliated sheets are at 350.32 cm^{-1} and 416.41 cm^{-1} while those of the bulk are at 349 cm^{-1} and 419.06 cm^{-1}, respectively. The prominent low-energy phonon mode is represented by E^1_{2g} (Γ), whereas, the high-energy phonon mode is represented by A_{1g} (Γ). The difference between the wavenumbers corresponding to E^1_{2g} (Γ) and A_{1g} (Γ) modes is found to be low for exfoliated WS_2 crystal in comparison to that of bulk—thereby validating the exfoliation [17]. Likewise, to confirm the exfoliation process, the phonon lifetimes of both bulk and exfoliated sheets were calculated using energy time uncertainty relation [18]. For bulk, it was 0.91 ps whereas for exfoliated sheets, it was 0.62 ps for A_{1g} (Γ) mode. As A_{1g} (Γ) mode implies out-of-plane vibration, that is, vibration along *c*-axis of the crystal, decrease of phonon lifetime in exfoliated sheets implies that exfoliation occurs along the *c*-axis. This further validates exfoliation of bulk WS_2.

4.3.3 Electrical characteristics

4.3.3.1 Current-voltage (*I*–*V*) characteristics of the un-treated resistive unit

The *I*–*V* characteristic of a representative resistive unit before introduction of noise is presented in **Fig. 4.2(d)**. Linear characteristics of the unit was observed with current in the nA region [3, 19]. A small difference in current value may be observed for different

resistive units prepared in the same manner. This is due to the uneven deposition of WS_2 nanosheets on the electrodes.

4.3.3.2 *I–V* characteristics of a resistive unit at different fabrication stage

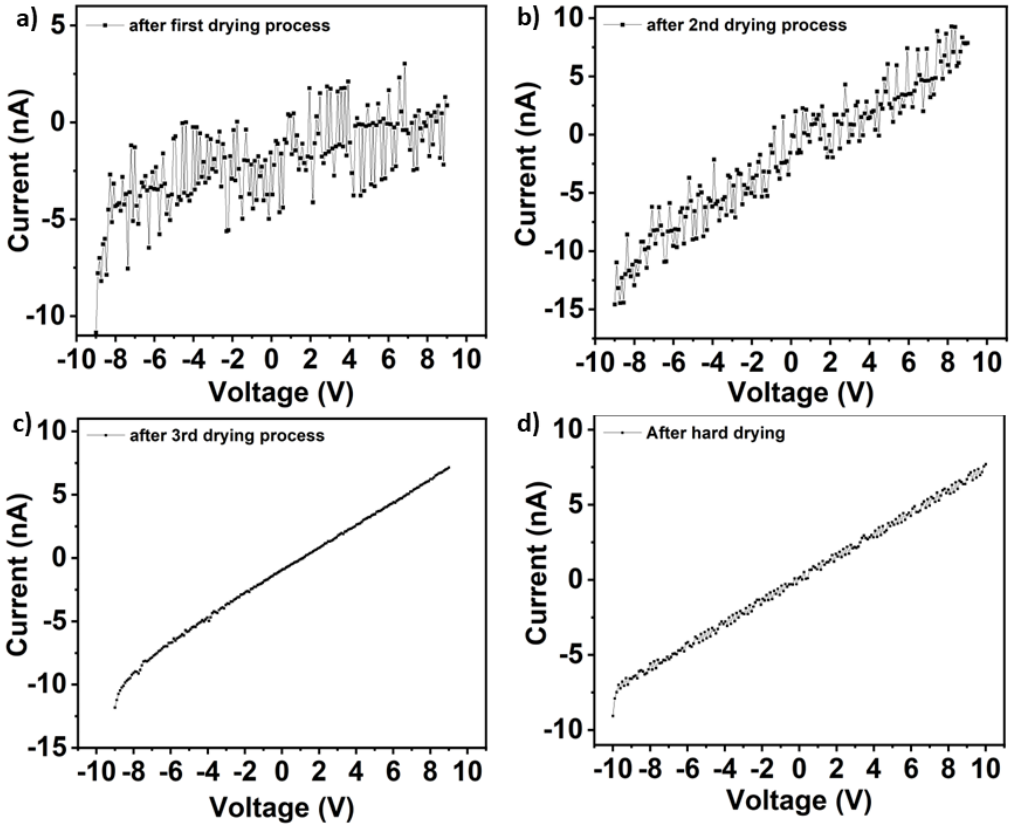

Fig.4.3. *I–V* characteristics of WS_2 based resistive unit after each drop casting and drying step. **(a)** After 1st drop caste and drying. At this stage, the system generated a random noise **(b)** After 2nd drop cast and drying process. At this preparation stage, enhancement of linearity in the current-voltage characteristics of the resistive unit was observed, however the system was coupled with a random noise **(c)** After 3rd drop caste and drying process. At this stage, the resistive system showed linear behaviour without any noise coupled to it. **(d)** After hard drying. At this stage $1/f$ noise was coupled to the system.

The change in the *I–V* characteristics of a randomly selected unit at every fabrication stage is presented in **Fig 4.3(a)–(d)**. It was observed that with every drop-casting and drying process, the current in the unit had improved. After drop casting and drying for the third time, the fabrication process was completed. However, further drying introduced fluctuations in the *I-V* characteristics of the system. This post-fabrication process was introduced to eliminate the effect of improper drop-casting mediated electrical fluctuations. **Fig. 4.3(d)** presents *I-V* characteristics of the noise coupled resistive unit. The noise-coupled resistive units were further irradiated using lasers having different centre

wavelengths, ensuring same power. For different centre wavelengths, different resistive units were used to eliminate interference associated with multiple laser irradiations.

4.3.3.3 Nature of the induced noise

Fig **4.4(a)** and **4.4(b)** show the power spectral density (PSD) of the current noise in two different resistive units named as X1 and X2 in the frequency range 0.01 to 10 Hz. The PSDs were compared to the ideal $^1/_f$ noise. It was observed that the linear fitted curves of power spectral density have $^1/_f$ dependence and follows $^1/_{f^\beta}$ behaviour, where β is the absolute value of the slopes of PSD vs frequency graphs. The value of β in X1 and X2 were found to be 1.073 ± 0.029 and 0.994 ± 0.014, respectively. The average value of β was approximately equal to 1. Therefore, the induced noise is $^1/_f$ dependent low frequency noise [20].

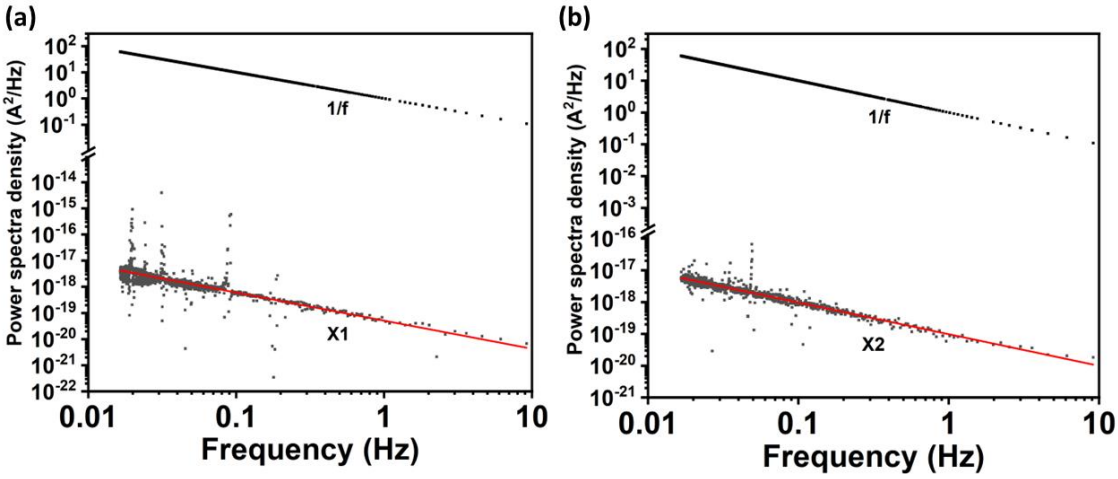

Fig.4.4. Power spectral density (PSD) vs. frequency graph of resistive units showing $^1/_{f^\beta}$ behavior. It is compared with ideal $^1/_f$ noise. Linear fitting performed on the PSDs of resistive units shows $^1/_f$ dependence **(a)** PSD of X1, where β = 1.073 ± 0.029 **(b)** PSD of X2, where β = 0.994 ± 0.014.

4.3.3.4 Effect of different laser sources on electrical characteristics of WS_2/Cu system

Three different resistive units coupled with the low frequency noise was prepared for laser irradiation. All the laser sources had near-perfect emission spectra with emission peaks centered at 650 nm (red laser), 532 nm (green laser), and 400 nm (blue laser). The resistive units before irradiation with red, green, and blue lasers are termed as WR, WG, and WB and after irradiation with red, green, and blue lasers are termed as R, G, and B respectively. *I–V* characteristics of them are displayed in **Fig. 4.5(a)–(f)**. The peak-to-peak fluctuation of current-voltage in WR was 14 nA (**Fig. 4.5(a)**). After irradiation with red laser, it was found to be ~ 28 nA (**Fig 4.5(d)**), achieving a two-fold increase in the current-voltage fluctuations. In WG, the peak-to-peak fluctuation in *I-V* characteristics was 12 nA (**Fig. 4.5(b)**), and after irradiation with green laser, it was found to be 60 nA. Hence, the intensity of the fluctuations was augmented five times in G compared to that of the original, as shown in **Fig. 4.5(e)**. The peak-to-peak fluctuation in *I-V* characteristics for WB was 13 nA (**Fig. 4.5(c)**), and after irradiation, it reached 35 nA. Hence, the intensity

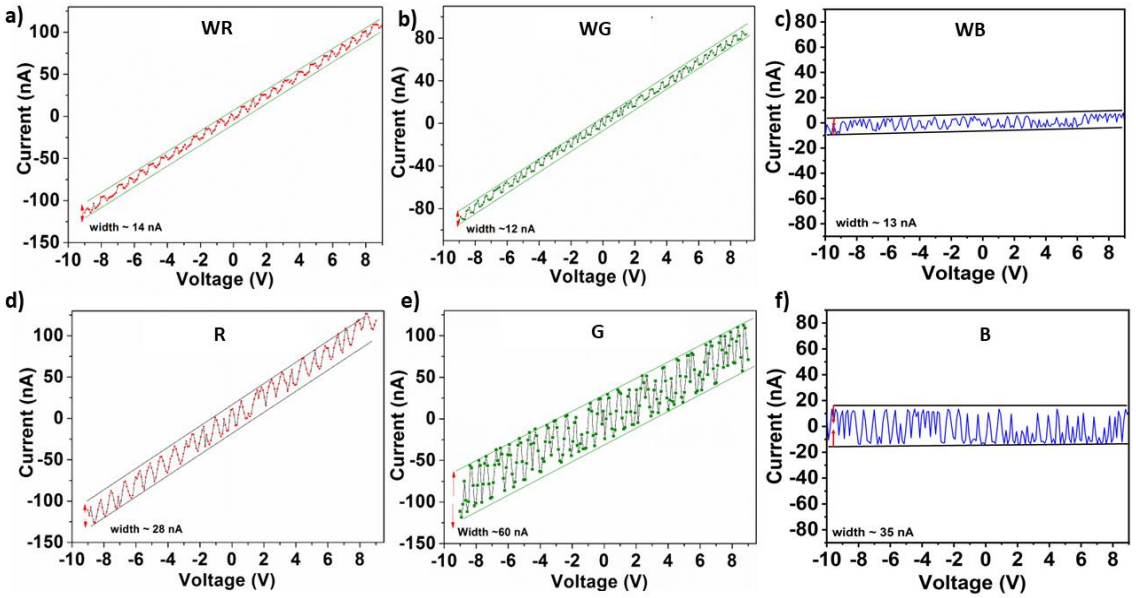

Fig.4.5. *I–V* characteristics of WS_2 nanosheets based resistive unit before irradiation with **(a)** red laser denoted by WR **(b)** green laser denoted by WG **(c)** blue laser denoted by WB. The peak-to-peak current-voltage fluctuation in WR, WG and WB are 14 nA, 12 nA and 13 nA respectively. *I− V* characteristics of WS_2 nanosheets based resistive unit after irradiation with **(a)** red laser denoted by R **(b)** green laser denoted by G **(c)** blue laser denoted by B. The peak-to-peak current fluctuation in R, G and B are 28 nA, 60 nA and 35 nA respectively.

of the fluctuations increased 2.7 times in B compared to that of the original, as shown in **Fig. 4.5(f)**.

The slope of the *I–V* characteristics provides the idea of linear conductance. The rise in the slope implies an increase in the conductance, while a decrease in the slope implies a reduction in the conductance. To determine the effect of laser irradiation on the linear conductance, two datasets of *I–V* characteristics before and after irradiation with each laser source were taken. **Fig. 4.6(a)** and **Fig. 4.6(b)** shows the linearly fitted *I–V* characteristics of the resistive units before irradiation with a red laser. They are denoted by S1 and S2. **Fig. 4.6(c)** and **Fig. 4.6(d)** shows the linear fitted *I–V* characteristics of the resistive units after irradiation with a red laser. They are denoted by Sr1 and Sr2. Similarly, **Fig. 4.7(a)–(d)** are the linear fitted *I–V* characteristics of the resistive units before (S3 and S4) and after (Sg1 and Sg2) irradiation with a green laser respectively. **Fig. 4.8(a)–(d)** shows the linear fitted *I–V* characteristics of the resistive units before (S5 and S6) and

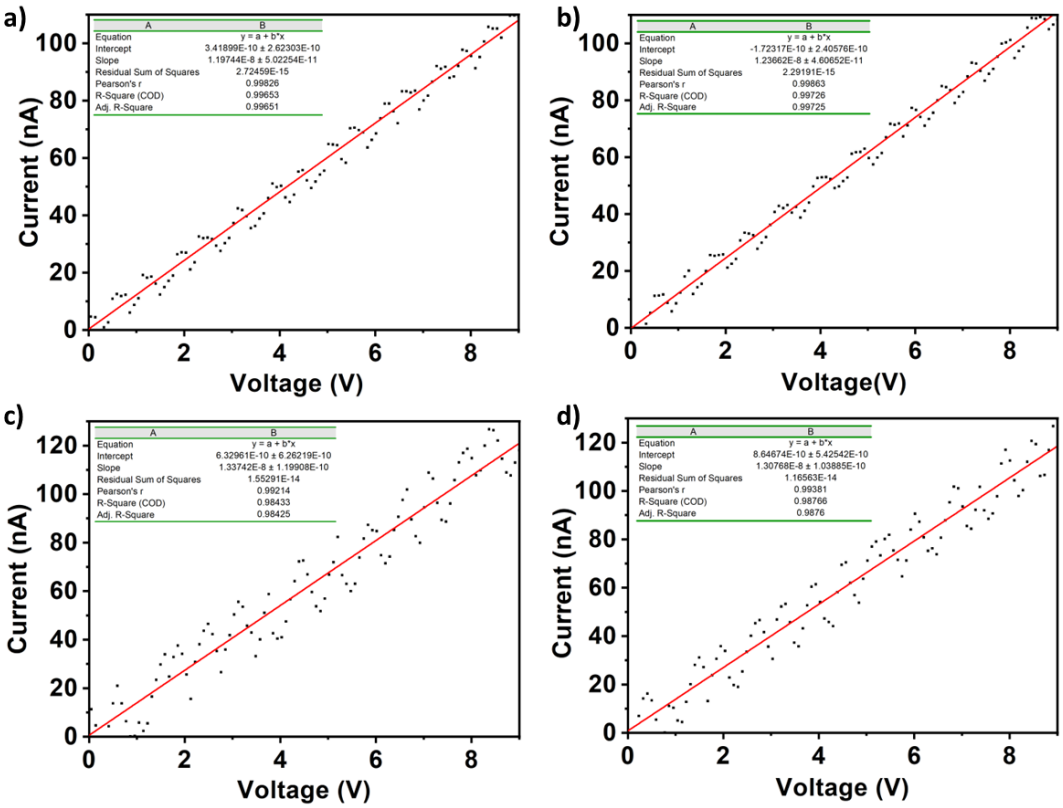

Fig.4.6. Linear fitting performed on *I−V* characteristics of resistive units **(a)** S1, before irradiation with a red laser, conductance (C)=1.19 x 10^{-8} S **(b)** S2, before irradiation with a red laser, C= 1.23 x 10^{-8} S **(c)** Sr1, after irradiation with a red laser, C= 1.33 x 10^{-8} S **(d)** Sr2, after irradiation with a red laser, C=1.30 x 10^{-8} S.

after (Sb1 and Sb2) irradiation with a blue laser respectively. The average value of conductance (C) of S1, S2, Sr1 and Sr2 is 1.27 x 10^{-8} S; that of S3, S4, Sg1 and Sg2 is 9.67 x 10^{-9} S. Similarly, for S5, S6, Sb1 and Sb2 is 5.74 x 10^{-10} S. The standard deviations of the conductance for all the 3 sets were found to be 6.41 x 10^{-10} S, 1.60 x10^{-10} S and 2.04

x10^{-10} S respectively. The results imply that the change in the conductance of the noise coupled resistive units due to laser-irradiation is of the order of 10^{-10} S. It is also noticeable that the enhancement of the fluctuations depends on the laser frequency. However, further investigations are required to have better understanding in this direction.

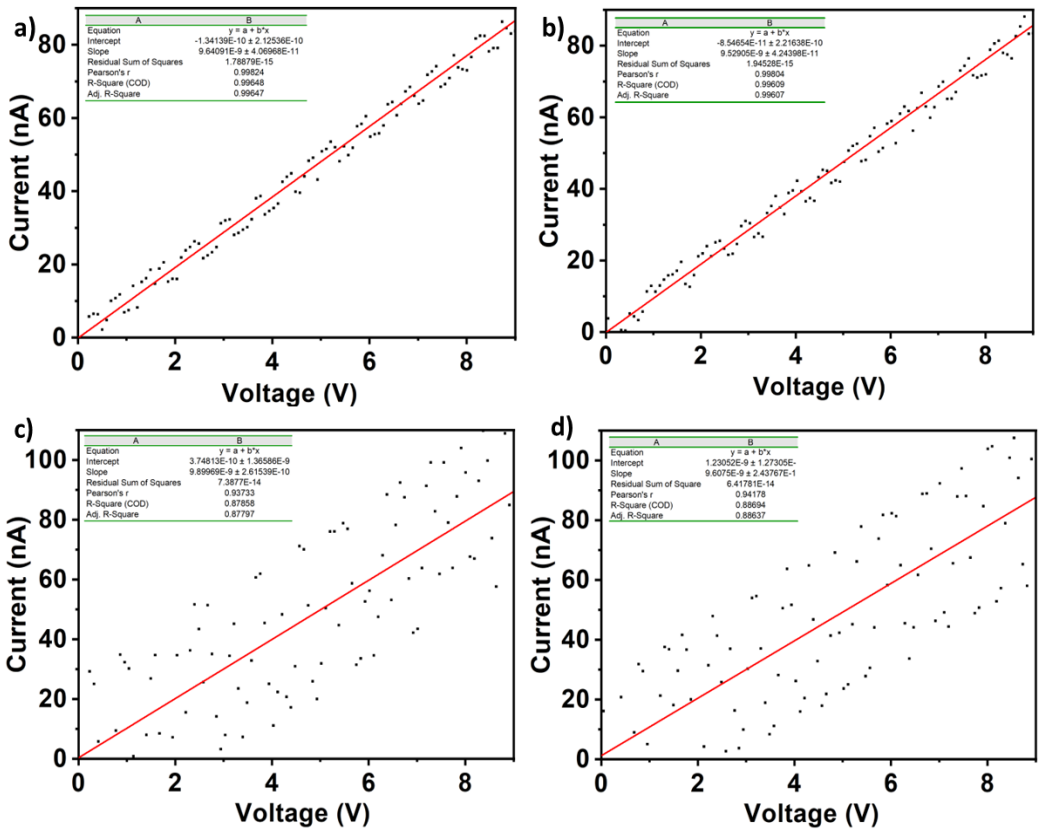

Fig.4.7. Linear fitting performed on *I*−*V* characteristics of resistive units **(a)** S3, before irradiation with a green laser, conductance (C)=9.64 x 10^{-9} S **(b)** S4, before irradiation with a green laser, C= 9.52 x 10^{-9} S **(c)** Sg1, after irradiation with a green laser, C= 9.89 × 10^{-9} S (d) Sg2, after irradiation with a green laser, C=9.60 x 10^{-9} S.

Then, the resistive units were characterized under different laser intensity. The intensity of the lasers was controlled using a pair of polarizer and analyser. The experimental setup designed for this investigation is shown in **Fig 4.9**. Effect of intensity varied laser irradiation on the resistive unit coupled with noise is presented in **Fig. 4.10(a)**. The peak-to-peak value of the fluctuations in the *I-V* characteristics vs. intensity of the laser illumination is plotted. It is observed that at first there is an increase in fluctuations with an increase in laser intensity in the noise coupled resistive system. Then after reaching a threshold, there is a decrease in fluctuations with an increase in intensity. This implies that current fluctuation in the system is intensity dependent.

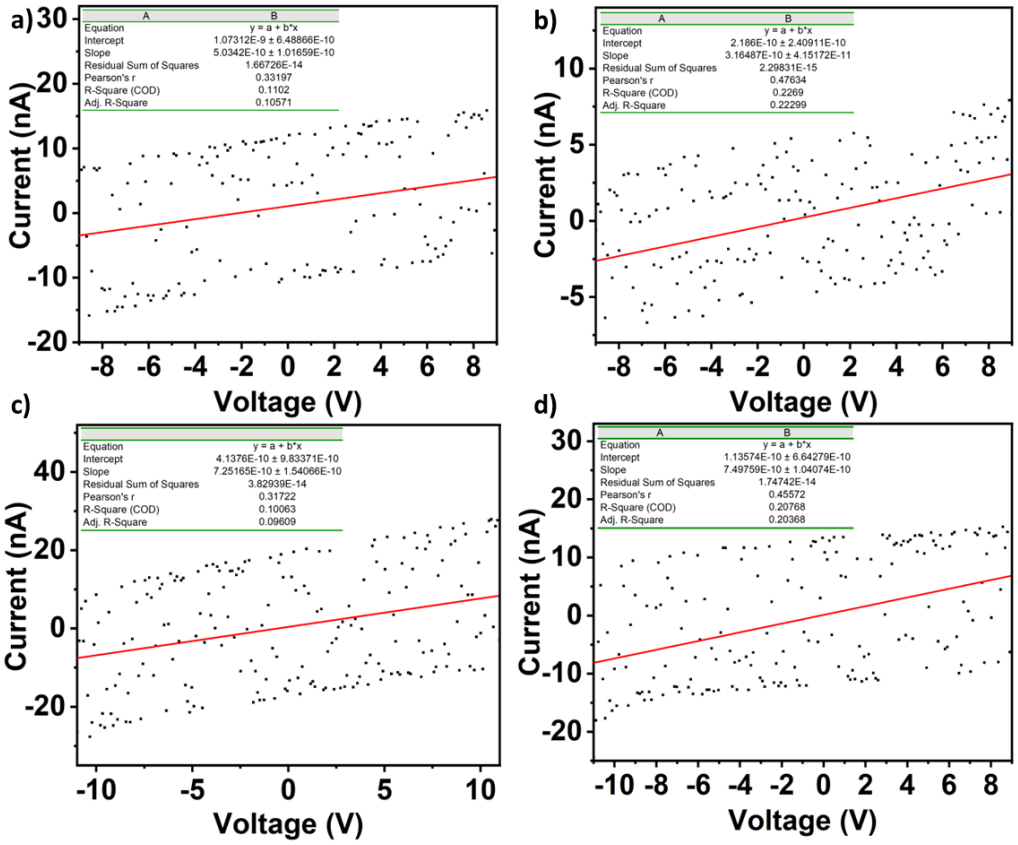

Fig.4.8. Linear fitting performed on *I*−*V* characteristics of resistive units **(a)** S5, before irradiation with blue laser, conductance (C)=5.03 x 10^{-10} S **(b)** S6, before irradiation with blue laser, C= 3.16 x 10^{-10} S **(c)** Sb1, after irradiation with blue laser, C= 7.25 x 10^{-10} S (d) Sb2, after irradiation with blue laser, C=7.49 x 10^{-10} S.

The effect of the laser can be clearly seen in the *I*–*t* characteristics of the resistive unit. **Fig 4.10(b)** shows the *I*–*t* characteristics of a resistive unit before and after irradiation with the green laser. An enhancement in the amplitude of the noise was observed when the laser was switched on and vice versa. This behavior also supports the amplitude fluctuations observed in the *I*–*V* characteristics of the resistive unit.

The obtained PSD suggests that the current noise is $^{1}/_{f}$ dependent Morrison [21] suggested that the charges trapped in double layers formed at interfaces, dislocations, and grain boundaries can give rise to $^{1}/_{f}$ noise. He explained the possibility of both carrier density fluctuations and mobility fluctuations for $^{1}/_{f}$ noise generation. In a recent study, it was found that carrier number fluctuations (CNF) govern the low frequency in monolayer WS_2 field-effect transistors (FET) on Si/SiO_2 substrates [20]. Similarly,

Sharma *et al.* [22] suggest the same for single and few layer MoS_2 based FETs. However, Sangwan *et al.* [23] explained the low frequency (LF) noise in single layer MoS_2 FET using Hooge's mobility fluctuations (HMF). Then, Renteria *et al.* [24] explained the low frequency noise in freshly fabricated and aged MoS_2 FET with McWhorter model of the CNF. Interestingly in a ~ 40 nm thick MoS_2 FET, Na *et al.* [25] used both CNF and HMF models to explain the results. Thus, different report suggests dissimilar explanations for similar electronic systems. Such diversified explanations for LF noise in similar devices suggest the limitations on the understanding of LF noise generation.

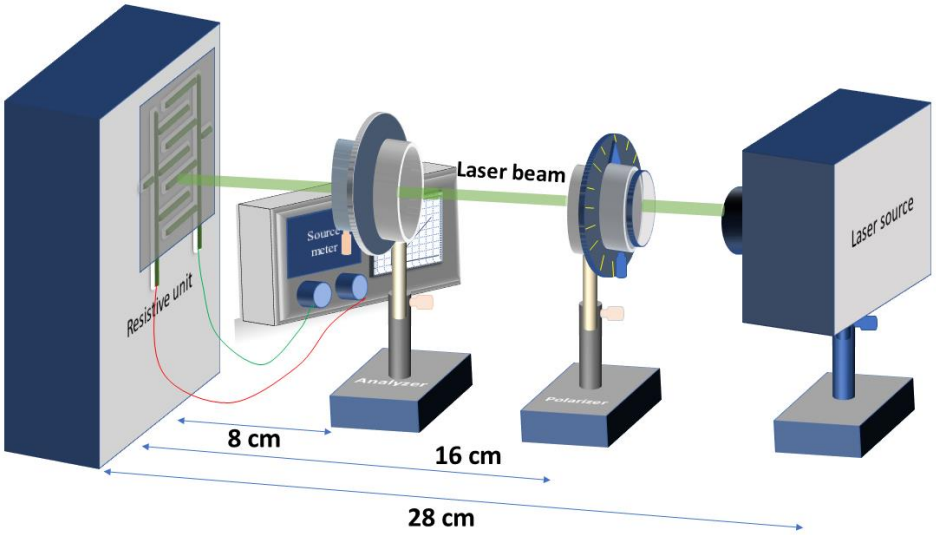

Fig.4.9. Schematic of the experimental set-up for performing laser intensity varied electrical analysis of nanostructured WS_2 based system.

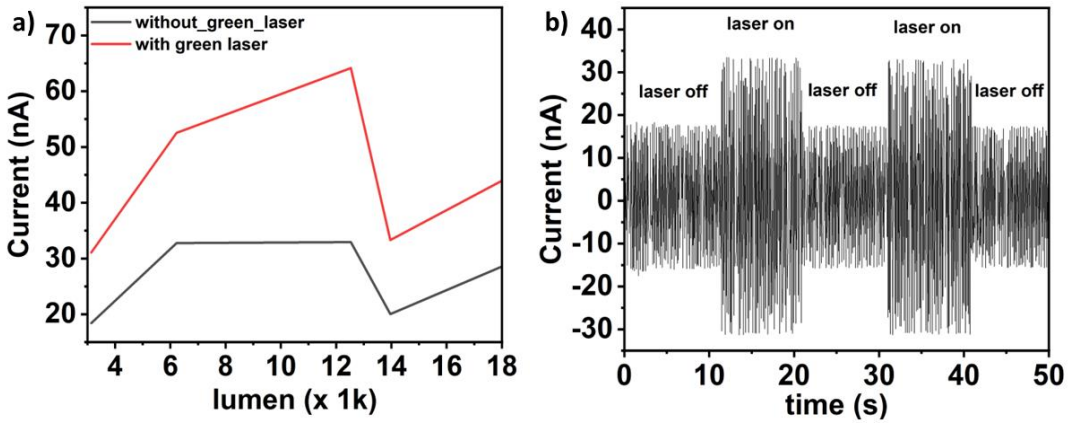

Fig.4.10. (a) Variation of peak-to-peak current fluctuation with change in laser intensity. The peak-to-peak current fluctuations increase with an increase in intensity; attains a maximum and then decreases with an increase in intensity **(b)** Current-time (*I-t*) characteristics of the resistive system coupled with noise before and after the laser treatment. The amplitude of the fluctuation increases when the laser is switched on and returned to its original amplitude when the laser is switched off.

WS_2 is a photoconductive material [3, 26-29]. Its electronic bandgap lies in between 1.32 and 2.03 eV [30]. Therefore, whenever WS_2 based electronic system is irradiated with visible light, generation of (*e*-*h*) pair takes place and hence the photo-current. Therefore, amplitude rise in *I*-*V* and *I*-*t* fluctuations were observed for all the laser lines. The fluctuations evident in the *I*-*V* curve denote the presence of negative differential resistance in the WS_2 nanosheet/Cu electrode system. Negative resistance suggests the formation of defect states and charge trapping at defects/imperfections and consequent carrier instability in the system [31,32]. Therefore, the observed phenomenon of 1/f noise can be ascribed to formation of defect states and carrier instability.

Experimental validation has substantiated that green laser irradiation can also induce the formation of Sulfur vacancies which can give rise to defect states on WS_2 nanosheets [33]. The more the intensity, the more the number of vacancies and subsequent increase in the current. Again, after green laser irradiation, it was observed that current noise, while initially ascending, reaches a threshold beyond which it undergoes a decline. This intriguing behavior can be attributed to the local oxidation induced by green laser irradiation. Local oxidation forms a tungsten-oxide dominated WS_2 nanosystem[33]. The ensuing oxide residuals gradually assert dominance, effecting the current gain.

The current-time (*I*–*t*) characteristics of the resistive system imply that the enhancement in the current is reversible and can be optimized with the help of laser irradiation. Therefore, this scheme can be used as a noise generator which can provide noise of required intensity in an *in situ* manner. This attribute can be applied to stochastic resonance-based sensing devices [34] to detect weak signals. The proposed scheme can be easily integrated into other electronic devices as well.

4.4 Conclusion

The chapter mainly focuses on two aspects *viz.* development of a WS_2 nanosheet/Cu electrode system coupled with noise and study the electrical characteristics of the same in the presence of laser irradiation. A co-solvent (mixture of isopropanol and acetone) was used to exfoliate the bulk WS_2 flakes. The exfoliated WS_2 nanosheets were drop-casted onto the finger-like Cu electrodes. The development of the resistive unit was examined at every step of the fabrication process. It was observed that the electrical behaviour of the system got improved with each drop casting and drying process. It was interesting to find

that the post-fabrication hard drying of the system introduced fluctuations in the *I-V* characteristics of the system. The power spectral density versus frequency spectra of the resistive system confirmed the formation of $^{1}/_{f}$ dependent noise. The *I–t* characteristics clearly showed the noise present in the system and enhancement of the noise with laser irradiation. The effect of laser irradiation on the linear conductance of the system was investigated by performing linear fitting of the *I–V* characteristics of the system. This shows that laser irradiation may change the linear conductance by the order of 10^{-10} S. It was observed that the noise enhancement is intensity dependent. The electrical attributes of the resistive unit suggest that it can be used as an *in situ* noise generator in sensing devices, where noise is used to detect weak signals. As the resistive system is lightweight and its arrangements can be easily integrated with other electronic components, it has the potential to replace bulky noise generators in weak signal detection devices.

References

[1] Splendiani, A., Sun, L., Zhang, Y., Li, T., Kim, J., Chim, C.Y., Galli, G. and Wang, F. Emerging photoluminescence in monolayer MoS_2. *Nano Letters*, 10(4): 1271-1275, 2010.

[2] Lee, H.S., Min, S.W., Chang, Y.G., Park, M.K., Nam, T., Kim, H., Kim, J.H., Ryu, S. and Im, S. MoS_2 nanosheet phototransistors with thickness-modulated optical energy gap. *Nano Letters*, 12(7): 3695-3700, 2012.

[3] Perea-López, N., Elías, A.L., Berkdemir, A., Castro-Beltran, A., Gutiérrez, H.R., Feng, S., Lv, R., Hayashi, T., López-Urías, F., Ghosh, S. and Muchharla, B. Photosensor device based on few-layered WS_2 films. *Advanced Functional Materials*, 23(44): 5511-5517, 2013.

[4] Choi, W., Cho, M.Y., Konar, A., Lee, J.H., Cha, G.B., Hong, S.C., Kim, S., Kim, J., Jena, D., Joo, J. and Kim, S. High-detectivity multilayer MoS_2 phototransistors with spectral response from ultraviolet to infrared. *Advanced Materials*, 24(43): 5832-5836, 2012.

[5] Dodda, A., Oberoi, A., Sebastian, A., Choudhury, T.H., Redwing, J.M. and Das, S. Stochastic resonance in MoS_2 photodetector. *Nature Communications*, 11(1): 1-11, 2020.

[6] Fauve, S. and Heslot, F. Stochastic resonance in a bistable system. *Physics Letters A*, 97(1-2): 5-7, 1983.

[7] Hibbs, A.D., Singsaas, A.L., Jacobs, E.W., Bulsara, A.R., Bekkedahl, J.J. and Moss, F. Stochastic resonance in a superconducting loop with a Josephson junction. *Journal of Applied Physics*, 77(6): 2582-2590, 1995.

[8] Hakamata, Y., Ohno, Y., Maehashi, K., Inoue, K. and Matsumoto, K. Robust noise characteristics in carbon nanotube transistors based on stochastic resonance and their summing networks. *Japanese Journal of Applied Physics*, 50(6S): 06GE03, 2011.

[9] Kawahara, T., Yamaguchi, S., Maehashi, K., Ohno, Y., Matsumoto, K. and Kawai, T. Robust noise modulation of nonlinearity in carbon nanotube field-effect transistors. *Japanese Journal of Applied Physics*, 49(2S): 02BD11, 2010.

[10] Lee, I., Liu, X., Zhou, C. and Kosko, B. Noise-enhanced detection of subthreshold signals with carbon nanotubes. *IEEE Transactions on Nanotechnology*, 5(6): 613-627, 2006.

[11] Kufer, D. and Konstantatos, G. Highly sensitive, encapsulated MoS_2 photodetector with gate controllable gain and speed. *Nano Letters*, 15(11): 7307-7313, 2015.

[12] Lv, Q., Yan, F., Wei, X. and Wang, K. High-performance, self-driven photodetector based on graphene sandwiched GaSe/WS_2 heterojunction. *Advanced Optical Materials*, 6(2): 1700490, 2018.

[13] Hirano, Y., Segawa, Y., Kawai, T. and Matsumoto, T. Stochastic resonance in a molecular redox circuit. *The Journal of Physical Chemistry C*, 117(1): 140-145, 2013.

[14] Hirano, Y., Segawa, Y., Kuroda-Sowa, T., Kawai, T. and Matsumoto, T. Conductance with stochastic resonance in Mn_{12} redox network without tuning. *Applied Physics Letters*, 104(23): 233104, 2014.

[15] Bao, J., Otsuka, Y., Etoh, R., Usami, Y. and Matsumoto, T. Local-field-induced current noise in shape-limited self-doped polyaniline. *Nanotechnology*, 31(36): 365203, 2020.

[16] Fujii, H., Setiadi, A., Kuwahara, Y. and Akai-Kasaya, M. Single walled carbon nanotube-based stochastic resonance device with molecular self-noise source. *Applied Physics Letters*, 111(13): 133501, 2017.

[17] Berkdemir, A., Gutiérrez, H.R., Botello-Méndez, A.R., Perea-López, N., Elías, A.L., Chia, C.I., Wang, B., Crespi, V.H., López-Urías, F., Charlier, J.C. and Terrones, H. Identification of individual and few layers of WS_2 using Raman Spectroscopy. *Scientific Reports*, 3(1): 1-8, 2013.

[18] Cuscó, R., Alarcón-Lladó, E., Ibanez, J., Artús, L., Jiménez, J., Wang, B. and Callahan, M.J. Temperature dependence of Raman scattering in ZnO. *Physical Review B*, 75(16): 165202, 2007.

[19] Neog, A., Deb, S. and Biswas, R. Atypical electrical behavior of few layered WS_2 nanosheets based platform subject to heavy metal ion treatment. *Materials Letters*, 268: 127597, 2020.

[20] Joo, M.K., Yun, Y., Yun, S., Lee, Y.H. and Suh, D. Strong Coulomb scattering effects on low frequency noise in monolayer WS_2 field-effect transistors. *Applied Physics Letters*, 109(15): 153102, 2016.

[21] Morrison, S.R. 1/f Noise from levels in a linear or planar array: Dislocations in metals. *Canadian Journal of Physics*, 71(3-4): 147-151, 1993.

[22] Sharma, D., Motayed, A., Shah, P.B., Amani, M., Georgieva, M., Glen Birdwell, A., Dubey, M., Li, Q. and Davydov, A.V. Transfer characteristics and low-frequency noise in single-and multi-layer MoS_2 field-effect transistors. *Applied Physics Letters*, 107(16): 162102, 2015.

[23] Sangwan, V.K., Arnold, H.N., Jariwala, D., Marks, T.J., Lauhon, L.J. and Hersam, M.C. Low-frequency electronic noise in single-layer MoS_2 transistors. *Nano Letters*, 13(9): 4351-4355, 2013.

[24] Renteria, J., Samnakay, R., Rumyantsev, S.L., Jiang, C., Goli, P., Shur, M.S. and Balandin, A.A. Low-frequency 1/f noise in MoS_2 transistors: Relative contributions of the channel and contacts. *Applied Physics Letters*, 104(15): 153104, 2014.

[25] Na, J., Joo, M.K., Shin, M., Huh, J., Kim, J.S., Piao, M., Jin, J.E., Jang, H.K., Choi, H.J., Shim, J.H. and Kim, G.T. Low-frequency noise in multilayer MoS_2 field-effect transistors: the effect of high-k passivation. *Nanoscale*, 6(1): 433-441, 2014.

[26] Gao, W., Zhang, S., Zhang, F., Wen, P., Zhang, L., Sun, Y., Chen, H., Zheng, Z., Yang, M., Luo, D. and Huo, N. 2D WS_2 based asymmetric Schottky photodetector with high performance. *Advanced Electronic Materials*, 7(7): 2000964, 2021.

[27] Sik Hwang, W., Remskar, M., Yan, R., Protasenko, V., Tahy, K., Doo Chae, S., Zhao, P., Konar, A., Xing, H., Seabaugh, A. and Jena, D. Transistors with chemically synthesized layered semiconductor WS_2 exhibiting 105 room temperature modulation and ambipolar behavior. *Applied Physics Letters*, 101(1): 013107, 2012.

[28] Liu, L., Kumar, S.B., Ouyang, Y. and Guo, J. Performance limits of monolayer transition metal dichalcogenide transistors. *IEEE Transactions on Electron Devices*, 58(9): 3042-3047, 2011.

[29] Bangolla, H.K., Lee, Y.C., Shen, W.C., Ulaganathan, R.K., Sankar, R., Du, H.Y. and Chen, R.S. Photoconduction Properties in Tungsten Disulfide Nanostructures. *Nanomaterials*, 13(15): 2190, 2023.

[30] Gusakova, J., Wang, X., Shiau, L.L., Krivosheeva, A., Shaposhnikov, V., Borisenko, V., Gusakov, V. and Tay, B.K. Electronic properties of bulk and monolayer TMDs: theoretical study within DFT framework (GVJ-2e method). *Physica Status Solidi (A)*, 214(12): 1700218, 2017.

[31] Chang, W.H., Lu, C.I., Yang, T.H., Yang, S.T., Simbulan, K.B., Lin, C.P., Hsieh, S.H., Chen, J.H., Li, K.S., Chen, C.H. and Hou, T.H. Defect-engineered room temperature negative differential resistance in monolayer MoS_2 transistors. *Nanoscale Horizons*, 7(12): 1533-1539, 2022.

[32] Chen, Y.T., Santiago, S.R.M.S., Sharma, S., Wu, C.B., Chou, C.L., Chang, S.H., Chiu, K.C. and Shen, J.L. Resistive switching accompanied by negative differential resistance in cysteine-functionalized WS_2 quantum dots toward nonvolatile memory devices. *ACS Applied Nano Materials*, *5*(2): 2250-2257, 2022.

[33] Neog, A. and Biswas, R. Phase transition and formation of inorganic fullerene type nanostructure in WS_2 nanosheet system under laser excitation. *Scripta Materialia*, 216: 114729, 2022.

[34] Krauss, P., Metzner, C., Schilling, A., Schütz, C., Tziridis, K., Fabry, B. and Schulze, H. Adaptive stochastic resonance for unknown and variable input signals. *Scientific Reports*, 7(1): 1-8, 2017.